Sea Ice Treatment for Polar WRF*

Keith M. Hines[1], David H. Bromwich[1,2], Aaron B. Wilson[1,2], and William L. Chapman[3]

[1]Polar Meteorology Group, Byrd Polar Research Center, The Ohio State University, Columbus, Ohio
[2]Atmospheric Sciences Program, Department of Geography, The Ohio State University, Columbus, Ohio
[3]Department of Atmospheric Sciences, University of Illinois at Urbana-Champaign, Urbana, Illinois

1. Introduction

Simple specifications for the sea ice surface are inadequate for highly detailed mesoscale simulations of the Polar Regions. During winter, sensible and latent heat fluxes are concentrated at polynyas and along leads where cold atmosphere is exposed to relatively warm open water. The thickness of sea ice varies between the (primarily) seasonal pack ice near Antarctica, first-year Arctic ice, and multi-year Arctic ice. While a constant sea ice albedo may be a reasonable specification for the Antarctic region, it is unacceptable for the spring to autumn seasons of the Arctic Ocean, when the variability is similar to the absolute value (Perovich et al. 2007; Mills 2011). We became concerned with the specification of sea ice surface during the preparations for the Arctic System Reanalysis (ASR, Bromwich et al. 2010; http://polarmet.osu.edu/PolarMet/ASR.html).

The ASR will provide a high-resolution depiction in space (~10 km) and time (~3 hr) of Arctic weather and climate. See Fig. 1 for a depiction of a domain that has been used for development of the ASR. For the atmosphere, the polar-optimized version of the advanced research Weather Research and Forecasting model (WRF-ARW), known as "Polar WRF" will be employed in conjunction with 3D-Var data assimilation by WRF-Var. The land surface conditions will be represented with the Noah land surface model (LSM) with Arctic modifications. To do this properly, we need a good specification of the ocean surface conditions. Sea surface temperature can be easily obtained from datasets based upon satellite observations and other sources. The specification of the sea ice surface, however, requires more care. Thus, to specify the sea ice surface for the ASR, a set of procedures have been implemented into Polar WRF.

*Corresponding Author Address: Keith M. Hines, Polar Meteorology Group, Byrd Polar Research Center, The Ohio State University, 1090 Carmack Road, Columbus, OH 43210-1002, email: hines.91@osu.edu.

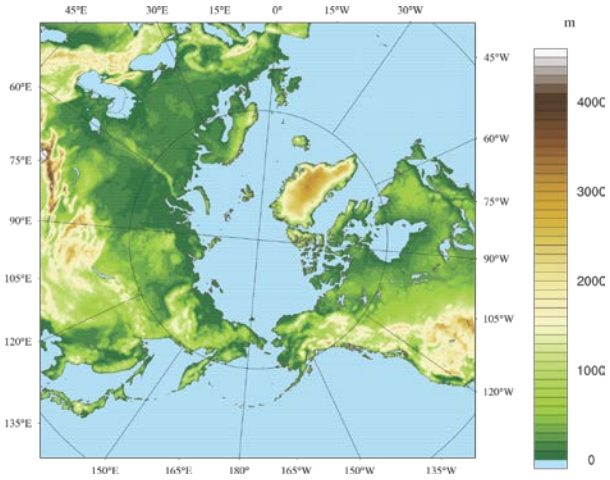

Figure 1. Domain of the Interim Arctic System Reanalysis at 30 km horizontal resolution.

2. Polar WRF

Work in past years by the Polar Meteorology Group (PMG) of The Ohio State University's Byrd Polar Research Center resulted in a polar-optimized version of the 5th generation Penn State/NCAR Mesoscale Model (MM5). Tests of "Polar MM5" showed that the model achieved a much improved performance for both Arctic and Antarctic regions (e.g., Bromwich et al. 2001). Later, a polar-optimized version was produced for WRF-ARW at the PMG, beginning with version 2 of the mesoscale model. Polar WRF (http://polarmet.osu.edu/PolarMet/pwrf.html) has been applied to multiple Arctic and Antarctic applications including for Greenland (Hines and Bromwich 2008); the Arctic Ocean (Bromwich et al. 2009), and Antarctic forecasting (Powers et al. 2010). More recently, it has been tested for northern Alaska land sites (Hines et al. 2011) and on an ASR domain (Wilson et al. 2011). It is also being used for the atmospheric component of the developing Arctic System Model (Cassano et al. 2011). Polar WRF is currently available for version 3.2.1 of WRF-ARW. Polar WRF will be updated for WRF-ARW version 3.3 during summer 2011.

3. Sea Ice in Polar WRF

The Arctic applications have revealed a need for an improved specification of sea ice conditions. Originally, the Noah LSM simply specified an ocean grid point as either sea ice or ocean water. Sea ice was 3 m thick with four equally spaced layers with prognostic temperature. Snow depth on sea ice was 0.05 m with mass equivalent to a water depth of 0.01 m. Sea ice albedo was also specified at a simple, uniform value.

Yet observations of the Arctic pack ice (e.g., Perovich et al. 2007) suggest large variability locally and seasonally within the pack ice domain (Fig. 2). For leads, the albedo may be only about 0.08. Melt pond albedo may vary from 0.4 for shallow ponds to 0.15 for deep ponds (Mills 2011). Over fresh snow, the albedo can exceed 0.85. Bare sea ice without snow or melt ponds typically has an albedo of about 0.65. The presence and characteristics of snow, melt ponds, and bare ice will vary over the course of a year, as was seen at the extensively observed Surface Heat Budget of the Arctic (SHEBA, Persson et al. 2002) camp during 1997/98. We wish to capture, at least to first order, the seasonal variability of the sea ice albedo in Polar WRF simulations.

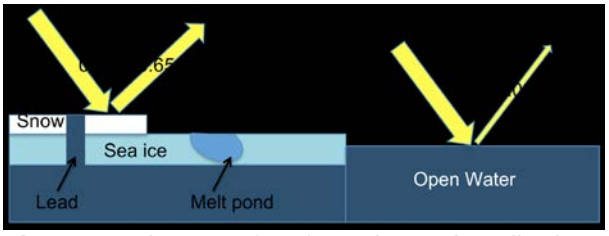

Figure 2. Diagram of surfaces impacting albedo for sea ice grid points. The albedo of fresh snow over sea ice is very high, while that for open water is very small. Bare ice and melt ponds have intermediate albedo values.

4. Detailed Procedure

The ice surface conditions in Polar WRF are treated with the option for specified fractional sea ice with the Noah land surface model in Polar WRF (Bromwich et al. 2009). The fractional sea ice capability is available in standard WRF beginning with WRF 3.1. Users need to specify the sea ice fraction. Relevant capabilities are added through supplements to Polar WRF for the WRF Preprocessing System (WPS) code. The supplements can work with sea ice concentrations from the bootstrap algorithm, Advanced Microwave Scanning Radiometer for EOS (AMSR-E), or the University of Illinois datasets. Horizontal resolutions of 25 km, 12.5 km, or 6.25 km are supported.

Within either the Noah or RUC LSMs, separate treatments are applied for the open-water and ice-covered fractions of pack ice grid points. The LSM is only called for the ice-covered fraction of the pack ice grid points. Accordingly, surface fluxes such as the sensible and latent heat fluxes are computed by the LSM for the ice fraction. In contrast, the atmospheric surface layer code computes the fluxes over open water. Wrapper programs for surface fields combine ice and water contributions with area-weighted averages. This is done for the surface fluxes and surface temperature.

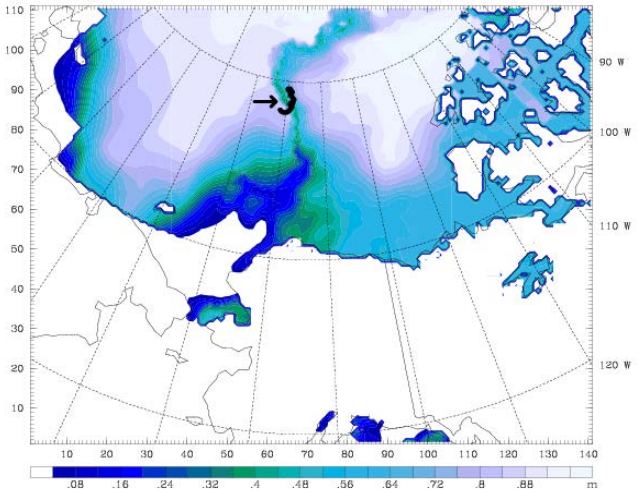

Figure 3. Color scale of average sea ice fraction during August 1998 from the bootstrap algorithm. The track of Ice Station SHEBA during August is shown next to the arrow. The domain shown was used for 25-km resolution Polar WRF simulations of selected SHEBA months.

While sea ice concentration has been routinely measured for decades from passive microwave remote sensing from satellites (See Fig. 3 for an example during August 1998), sea ice thickness is less easy to determine. However, through the use of satellite data and drifting buoys, the formation, movement, and disappearance of sea ice can be tracked, and this method has been used for the ASR. The fourth author worked with James Maslanik of the National Snow and Ice Data Center (NSIDC) to enable the estimation of sea ice age which is related to thickness (Maslanik et al. 2007). Platforms employed include daily satellite images acquired by the Scanning Multichannel Microwave Radiometer (SMMR), the Special Sensor Microwave/Imager (SSM/I), and the series of Advanced Very High Resolution Radiometer (AVHRR) sensors. Data at 25 km resolution are available up to June 2002. For more recent times, 6.25 km resolution AMSR-E

retrievals are employed. A sinusoidal annual cycle is imposed on derived sea ice thicknesses approximated from in-situ measurements. Sea ice concentration and thickness can be fed into Polar WRF surface boundary conditions through the supplemental WPS code.

Sea ice albedo in the ASR is represented through an annual Arctic cycle inspired by and simplified from the 5-stage Perovich et al. (2007) model of sea ice albedo. This is referred to as the PMG algorithm. Albedo is impacted through assumed behavior for snow cover and melt ponds. Prior to the onset of snow melt over sea ice, sea ice albedo is set at 0.82. For Wilson et al. (2011) and the ASR, onset of snow melt over sea ice is determined for 16 sectors of longitude each year from passive microwave through a dataset supplied by Mark Anderson of the University of Nebraska-Lincoln (Drobot and Anderson 2001). During a 30-day snow melt period, sea ice albedo decreases linearly to 0.5, analogous to the observed trend at SHEBA. During July, melt ponds are presumed to grow deeper and darker until they are represented as "open water" outside the ice fraction treated by the Noah LSM. The albedo of the remaining bare ice is set at 0.65 for early August. Between August 15th and September 4th, freeze-up occurs and the sea ice albedo increases linearly to 0.82. New datasets for ice freeze-up will make it possible to specify freeze-up each year based upon observations, rather than depending upon one given pattern taken from the 1998 SHEBA case.

For snow depth on sea ice, monthly values are based upon 1954-1991 observations at Russian sea ice stations (Warren et al. 1999) over the Arctic Ocean, along with additional constraints including Radionov et al.'s (1996) observations over first year ice.

5. Alternative sea ice Albedo (UIUC Algorithm)

An alternative method for representing sea ice albedo in WRF has been developed at the University of Illinois (UIUC) Department of Atmospheric Sciences. This method does not require assuming or specifying the times of snow melt, freeze-up, or melt-pond development. It is controlled by atmospheric temperature, surface temperature, and snow depth. It is more easily applied to simulations of future scenarios when times of snow melt or freeze-up will not be known. Furthermore, the method can represent synoptic timescale variations in albedo that are not captured by the season-based PMG algorithm.

Required inputs are snow depth on sea ice, the surface temperature and the near-surface atmospheric temperature. Where snow covers sea ice and (a) the surface temperature is below -5°C, the albedo is 0.80, (b) the surface temperature is 0°C, the albedo is 0.65, and (c) in between, the albedo is linear with surface temperature from 0.80 and 0.65. For ice without snow and (a) the surface temperature is below -5°C, the albedo is 0.65, otherwise if (b) the near-surface temperature is below 0°C, the albedo is 0.65, (c) the near-surface temperature is above 5°C, the albedo is 0.45, and (d) in between the albedo is linear with air temperature from 0.65 to 0.45. The fraction of snow cover increases with snow depth, with the snow fraction set at the ratio of snow depth to the sum of snow depth plus surface roughness. .

6. 1998 SHEBA Case

Figure 4 shows time series of albedo for April to September 1998 at SHEBA near the Beaufort Sea in the Arctic Ocean. The purple line shows average albedo measured by the SHEBA Ice Physics Group along a 200-m transect line including ice, melt ponds and leads. The purple line is impacted by leads, especially during late summer, so it tends to show reduced values. The blue line displays the local Atmospheric Surface Flux Group tower measurement (Persson et al. 2002). As only a small area is represented instantaneous tower values show large variability. There is also a diurnal cycle in the tower albedo displayed. Tower measurements become impacted by a melt pond during late June, resulting in a reduced albedo. Generally, the tower measurement is less impacted by leads and melt ponds, so it has larger albedo than the transect observations. Both of the model algorithms show a representation of the seasonal cycle with high albedo during spring and with the development of significant albedo reduction during summer.

The red line is the representation for the PMG seasonal algorithm that has seven stages (0.82, 0.82 to 0.50, 0.50, 0.50 to 0.65, 0.65, 0.65 to 0.82 and 0.82). Snow melt onset at SHEBA begins on 29 May and corresponds to the reduction in albedo from 0.82. WRF Noah only treats the ice fraction, not the open water fraction. Consequently, the treated albedo counter-intuitively increases from 0.5 to 0.65 during July as the melt ponds deepen and are eventually treated as "open water." The freeze-up occurs during the latter half of August until the albedo eventually returns to 0.82 on 4 September. The PMG algorithm values are closest to the transect observations during June. From late July to September the PMG algorithm is closest to the tower observations. The difference between the red and purple lines during late summer is probably due to leads, that are not part

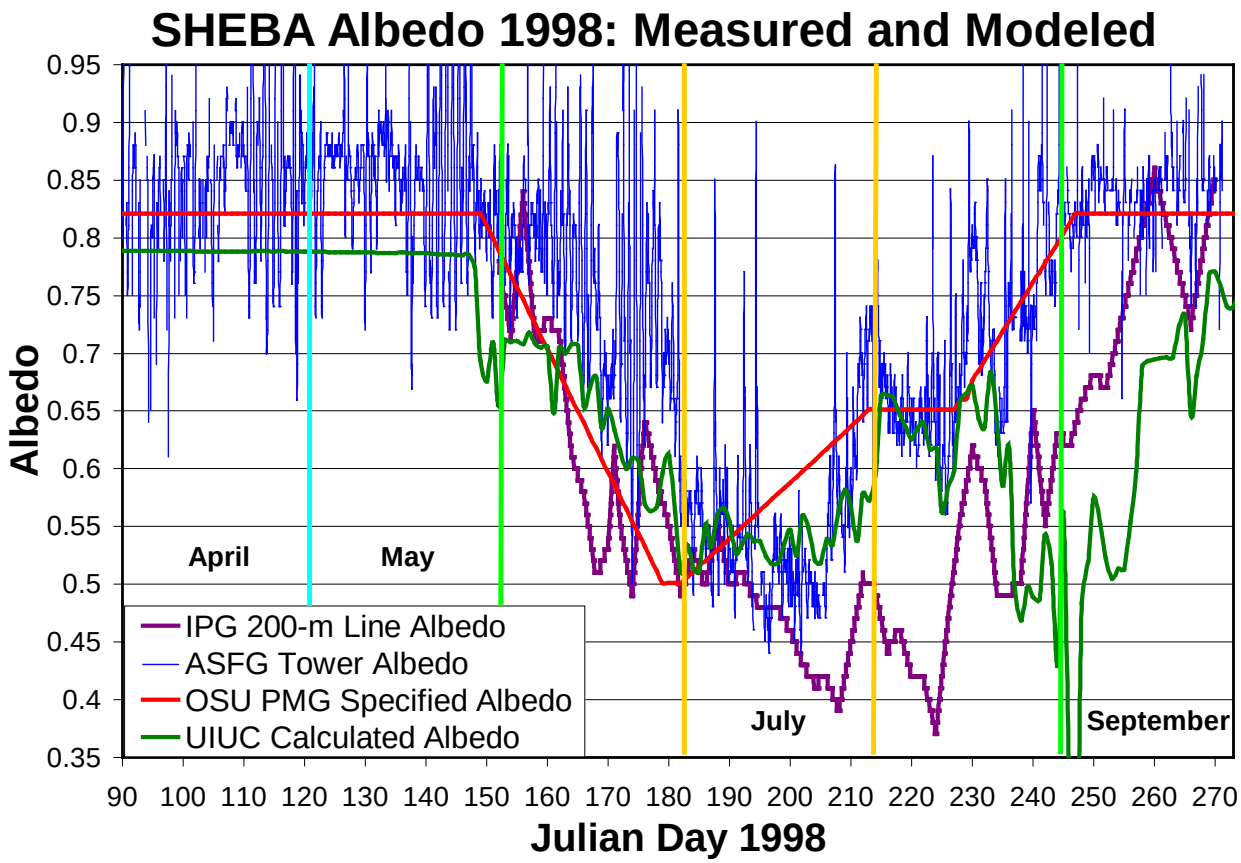

Figure 4. Time series of albedo (fraction) over sea ice during 1998 for observations from the SHEBA tower (blue), the 200-m SHEBA transect (purple), and modeled with the algorithms from the PMG (red) and UIUC (green).

of the ice fraction represented by WRF, but reduced the measured transect albedo. Since the modeled sea ice albedo is based upon SHEBA observations, it would be interesting to do a similar comparison of the PMG algorithm versus observations for an independent case. The Arctic Summer Cloud Ocean Study (ASCOS) observations during 2008 would provide a good test case.

The green line displays the sea ice albedo for the UIUC algorithm. It displays an area-average albedo interpolated to the drifting SHEBA site from model grid boxes with 60 km resolution. The incorporation of temperature allows the albedo to vary on shorter timescales. The displayed albedo has reduced values as the grid box averages are impacted by leads unlike the PMG values shown. Thus the albedo is about 0.78 during April rather than 0.8, the maximum possible value for snow-covered ice. The noticeable seasonal decay in albedo begins abruptly on 27 May. During June the UIUC values are larger than the PMG values and closer to the tower albedo measurements. The green line continues to reasonably agree with the tower albedo until mid August. Then, the green line is impacted by large expanses of open water within the 60 km grid boxes, so the values are much lower than observations from both the transect and the tower. The signature of fall freeze-up is delayed and less robust for the UIUC algorithm due to the continuing presence of leads during September. In summary, from the lines displayed in Fig. 4 it would be premature to select either the PMG or UIUC method as better than the other. Areal representativeness of the observations used for comparison remains an issue. More extensive tests would are required to evaluate the algorithms. However, Fig. 4 does display the ability of the PMG and UIUC methods to represent seasonal variability in Arctic sea ice albedo.

ACKNOWLEDGMENTS. This research is supported by NSF grants IPY-0733023 and ANT-1049089, along with the NSF support for the AMPS real-time Antarctic forecasting.

7. REFERENCES

Bromwich, D.H., J.J. Cassano, T. Klein, G. Heinemann, K.M. Hines, K. Steffen and J.E. Box, 2001: Mesoscale modeling of katabatic winds over Greenland with the Polar MM5. Mon. *Wea. Rev.*, **129,** 2290-2309.

Bromwich, D.H., K.M. Hines and L.-S. Bai, 2009: Development and testing of Polar Weather Research and Forecasting model: 2. Arctic Ocean. *J. Geophys. Res*., **114,** D08122, doi:10.1029/2008JD010300.

Bromwich, D., Y.-H. Kuo, M. Serreze, J. Walsh, L.S. Bai, M. Barlage, K. Hines, and A, Slater, 2010: Arctic System Reanalysis: Call for community involvement. *EOS Trans. AGU*, **91,** 13-14.

Cassano, J.J., M.E. Higgins, and M.W. Seefeldt, 2011: Performance of the Weather Research and Forecasting (WRF) model for month-long pan-Arctic Simulations. *Mon. Wea. Rev.*, **139,** in press.

Drobot, S., and M.R. Anderson, 2001: An improved method for determining snowmelt onset dates over Arctic seaice using scanning multichannel microwave radiometer and Special Sensor Microwave/Imager data. *J. Geophys. Res.*, **106,** 24,033-24,049.

Hines, K.M., and D.H. Bromwich, 2008: Development and testing of Polar WRF. Part I. Greenland Ice Sheet Meteorology. *Mon. Wea. Rev*., **136,** 1971-1989.

Hines, K.M., D.H. Bromwich, L.-S. Bai, M. Barlage, and A.G. Slater, 2011: Development and testing of Polar WRF. Part III. Arctic land. *J. Climate*, **24,** 26-48, doi: 10.1175/2010JCLI3460.1.

Maslanik, J.A., C. Fowler, J. Stroeve, S. Drobot, J. Zwally, D. Yi, and W. Emery, 2007: A younger, thinner Arctic ice cover: Increased potential for rapic, extensive sea-ice loss. *Geophys. Res. Lett.,* **34,** L24501, doi:10.1029/2007GL032043.

Mills, C.M., 2011: On the Weather Research and Forecasting model's treatment of sea ice albedo over the Arctic Ocean*. 10th Annual School of Earth, Society, and Environmental Research Review*, 25 February 2011, University of Illinois at Urbana-Champaign, Urbana, IL. [available at http://igloo.atmos.uiuc.edu/ASR/CMMills_poster_SESE_2011_FINAL.pdf]

Perovich, D.K., S.V. Nghiem, T. Markus and A. Schweiger, 2007: Seasonal evolution and interannual variability of the local solar energy absorbed by the Arctic sea ice–ocean system. *J. Geophys. Res*., **112,** C03005, doi:10.1029/2006JC003558.

Persson, P.O.G., C.W. Fairall, E.L. Andreas, P.S. Guest and D.K. Perovich, 2002: Measurements near the Atmospheric Surface Flux Group Tower at SHEBA: Near-surface conditions and surface energy budget. *J. Geophys. Res.*, **107,** 8045, doi:10.1029/2000JC000705.

Powers, J.G., S.M. Cavallo, and K.W. Manning, 2010: Improvements to radiation on upper-level WRF performance over the Antarctic. Preprints, *11th WRF Users' Workshop*, 21-25 June 2010, Boulder, CO, National Center for Atmospheric Research.

Radionov, V.F., N.N. Bryazgin, and Y.I. Aleksandrov,.1996: The snow cover of the Arctic Basin (in Russian). Gidrometeoizdat, 102 pp.

Warren, S.G., I.G. Rigor, and N. Unterseiner, V.F. Radionov, N.N. Bryazgin, and Y.I. Aleksandrov, 1999: Snow depth on Arctic sea ice. *J. Climate*, **12,** 1814-1829.

Wilson, A.B., D.H. Bromwich, and K.M. Hines, 2011: Evaluation of Polar WRF forecasts on the Arctic System Reanalysis domain. Part I. Surface and upper air analysis. *J. Geophys. Res*., **116,** D11112, doi:10.1029/2010JD01501.